Profiling ALACEs and Other Advances in Autonomous Subsurface Floats

R. E. DAVIS, J. T. SHERMAN, AND J. DUFOUR

Scripps Institution of Oceanography, La Jolla, California

(Manuscript received 6 October 1999, in final form 25 September 2000)

ABSTRACT

Over the past decade more than 1200 autonomous floats have been deployed worldwide. In addition to velocity as marked by lateral movement, many of these floats measured quantities like profiles of temperature and salinity, temperature microstructure, and time series of vertical velocity. The authors' laboratory's implementation of profile measurements in what is called a Profiling Autonomous Lagrangian Circulation Explorer is described. Biofouling and degradation of antifouling coatings on the conductivity sensor both cause drifts that mean accurate salinity measurements will depend on corrections based on known temperature–salinity relations. A second generation autonomous float called the Sounding Oceanographic Lagrangian Observer (SOLO) has been developed to provide enhanced reliability and to provide complete two-way depth control. A dual hydraulic-pneumatic buoyancy system reduces the energy cost of vertical cycling and buoyancy generation at the surface. A SOLO Vertical Current Meter has been found capable of measuring vertical velocity with errors of $O(3\ \text{m day}^{-1})$ on month timescales.

1. Introduction

Since the 1950s neutrally buoyant subsurface floats have been used to track ocean currents (Swallow 1955). Over the years an array of various floats have been in service, employing a number of tracking and operational techniques. The first subsurface current follower to be tracked at long range, the Sound Fixing and Ranging Float (SOFAR; Rossby and Webb 1970) float, was located using a low-frequency sound source on the float whose signal was tracked by multiple listening stations. The RAFOS (SOFAR spelled backward) float (Rossby et al. 1986) reverses this acoustic tracking with each float locating itself using signals received from multiple sound sources. The first autonomous float, the Autonomous Lagrangian Circulation Explorer (ALACE; Davis et al. 1992) operates without the need of acoustic tracking networks by repetitively cycling to the surface for satellite tracking and data relay. Eliminating acoustic tracking reduces operational costs, particularly when the float density is low, and allows results to be available rapidly, but gives up continuous tracking that may be desirable in narrow boundary currents or energetic eddy fields.

Since 1990 ALACE floats have been used to track ocean currents to depths down to 1.5 km (Davis et al. 1996; Davis 1998). Operationally, the float sinks to its neutral-buoyancy depth, drifts with the current, and after a programmed time (typically 5–30 days) increases its buoyancy by pumping oil into an external bladder in order to rise to the surface. It transmits data to Service Argos satellites over a 24-h interval, returns the oil to the internal bladder, and sinks again to its neutral-buoyancy depth. Service Argos reports a sequence of float surface positions and these are used to estimate the ascent and descent positions from which subsurface velocity, averaged over the submerged period, is computed. Cycling continues until the float fails; for a successful ALACE this occurs when battery energy is depleted after ~100 cycles.

The autonomous float's vertical ascent/descent cycle provides an ideal opportunity to measure profiles of various ocean properties like temperature and salinity at small additional cost. Our laboratory has, mainly as part of the World Ocean Circulation Experiment, deployed 290 temperature Profiling ALACEs (P-ALACEs) since 1991, and since 1994 we have set 95 conductivity–temperature–depth (CTD) profilers. With greater stored battery energy than an ALACE, the power-limited life of a P-ALACE is ~200 cycles. Measuring conductivity over long time spans has proven challenging. Biofouling issues and sensor longevity have contributed to sensor drift and calibration shifts. P-ALACE technology and performance is discussed in section 2.

An autonomous float's subsurface drifting interval provides an opportunity to measure vertical flow. Following the original concept of the Vertical Current Meter (VCM; Voorhis and Webb 1970), an autonomous float capable of measuring vertical velocity time series

Corresponding author address: Dr. Russ E. Davis, Physical Oceanography Research Division, 0230, Scripps Institution of Oceanography, University of California, 9500 Gilman Dr., La Jolla, CA 92093-0230.
E-mail: rdavis@ucsd.edu

over multiple seasons has been developed. This VCM float has yielded valuable information about internal waves and deep convection in the Labrador Sea, and may be capable of measuring upwelling occurring on the mesoscale or larger (section 3).

While over 1000 ALACEs have been successfully deployed, it has a number of design characteristics that are not optimal. 1) The original ALACE, whose hydraulic buoyancy engine is powered by a reciprocating pump, is unable to reduce its buoyancy while under high pressure. Consequently, while it can adjust its neutral buoyancy depth upward, an ALACE cannot adjust its depth downward without surfacing. 2) ALACE's internal oil bladder is subject to rupture under high acceleration loading such as might be experienced in shipping or on air deployment. 3) As described by Davis et al. (1992), a significant fraction of the ALACE energy budget is associated with pumping a relatively large volume of oil at the surface where its high-pressure pump is quite inefficient. 4) Perhaps most important, despite numerous improvements in manufacture and preparation, the original ALACE remained unreliable. For all these reasons, we have developed a second-generation float, the Sounding Oceanographic Lagrangian Observer (SOLO), which is described in section 4. The SOLO uses a single-stroke hydraulic pump that allows full up-down control, eliminates any internal oil bladder and whose simplicity should improve reliability. Additional buoyancy is efficiently generated at the surface by a low-pressure air pump filling an external pneumatic bladder.

2. Temperature and salinity profiling

All that is needed to convert an ALACE into a P-ALACE are sensors to measure the properties being profiled and changes to the controller program to store and relay profile data. The existing ALACE pressure sensor completes the instrumentation. Because profile data is likely to be of interest on time intervals less than those required for accurate large-scale velocity measurements, it is desirable that a profiling float be capable of cycling vertically many more times than an ALACE. For this reason and to support the increased energy used per cycle to transmit profile data, a P-ALACE is slightly larger than an ALACE to house an augmented lithium battery pack capable of delivering 4 MJ. For temperature and CTD versions, respectively, the pressure cases are 15 and 20 cm longer and masses are 25 and 27 kg. This increases the power-limited life to 200 cycles, making it possible for a temperature P-ALACE to measure temperature profiles for approximately the cost of an XBT, and allowing a CTD P-ALACE to measure a pair of temperature (T) and salinity (S) profiles for about 1.5 times this cost. In order to realize this potential for economical profiling, however, it is necessary that sensors be stable over the life of the float.

The P-ALACE temperature sensor for both temperature and CTD configurations is a very stable, 3-mm diameter YSI 46016 thermistor mounted in thermally conducting grease at the tip of a 10-cm-long stainless steel probe as pictured in Fig. 1. The probe and the associated electronics are calibrated against a secondary standard with an estimated precision of 0.005°C. The time constant of the probe was measured in dip tests into quiet water to be approximately 2 s.

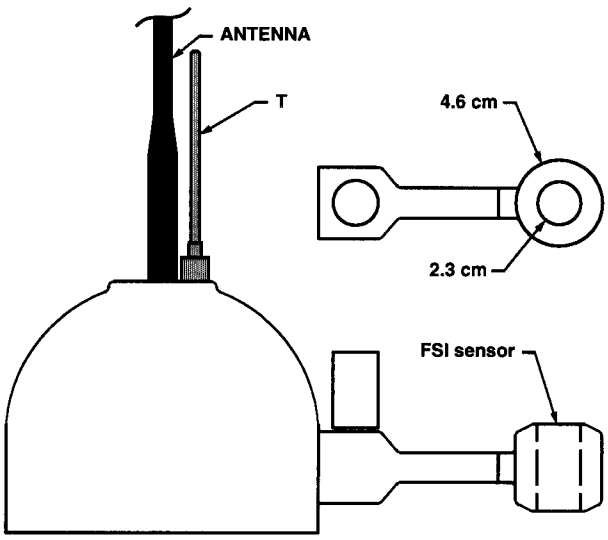

FIG. 1. The CTD P-ALACE top hemispherical end cap has an Argos antenna and temperature probe mounted on the top and an FSI inductive conductivity cell attached on the side. The FSI sensor is a torroid that contains the drive and sense coils. Measured conductivity is most sensitive to the water volume inside the torroid's hole but objects located within a 10-cm radius can cause salinity shifts of $O(0.01)$ psu.

A Paine 211-38-050-02 bonded strain-wire strain-gauge pressure sensor and port were retained from the ALACE. Profiling results indicate that the pressure sensor, which is mounted directly to the instrument end-cap, is subject to hysteresis errors of $O(5$ db) that far exceed what can be explained by simple temperature sensitivity of the sensor calibration. We attribute this error to a sensitivity to temperature gradients within the sensor induced when the sensor sees a changing temperature. The same problem was encountered in early SOLOs (see below) and has been circumvented by thermally isolating the sensor. During profiling, temperature and conductivity readings are taken every 2 s and these readings are averaged in situ over depth bins that typically expand from 2 or 5 m near the surface to 20 m at depth. It is these average values that are relayed through Argos.

The requirements for a P-ALACE conductivity sensor are long-term stability, low power consumption, good flushing at low speeds (typical ascent speed is 10–20 cm s^{-1}), and resistance to biological fouling. Commercial sensors include those using electrode and inductive sensing techniques. Both are characterized by a cell geometry with a pathlength, L, and cross-sectional area,

A, that measures a resistance, *R,* related to conductivity, *C,* by

$$R \sim L/AC. \quad (1)$$

Errors in measuring *C* arise from electronics drift, electrode resistance (which, crudely, is added to *R*), and changes of cell geometry. Performance degradation resulting from electrode resistance and passivation is eliminated in an inductive-sensing element. Shifts in geometry occur from pressure, temperature, corrosion, and biological fouling. By using stable materials (ceramics and glass) the effects of *P* and *T* on geometry can be minimized and well characterized, but biofouling is not easily eliminated. If *L* and *A* are characterized with the dimension λ, the fractional error in a conductivity measurement resulting from a dimensional change $\delta\lambda$ is $O(\delta\lambda/\lambda)$. If one assumes that biofouling is the primary concern and that it will perturb the cell dimensions by a given amount $\delta\lambda$ determined by biological growth rates, then cells with large dimensions λ should be more stable than small sensors.

Relative insensitivity to biofouling and an uncertainty about how electrode performance would be affected by biocides used to reduce fouling were the main factors leading to our selection of an inductive conductivity sensor. The inductive cell can be coated with a biocide to slow fouling, but, because this coating is fully exposed, the biocide must be expected to ablate and/or dissolve relatively quickly. This limits the period over which antifouling can be effective, and if the physical dimensions of the biocide coating change as it weathers, cell calibration can be expected to change in the opposite sense that growth on the cell will change it. In this respect a cell that can be isolated from the surrounding sea by shutters or by being enclosed in a pumped system, inside which slow biocide release can maintain high concentrations when the cell is not in use, may be preferred.

We have deployed 95 floats using the Falmouth Scientific Inc. (FSI) inductive cell model CSA-3 (Fougere 2000) mounted to the P-ALACE top cap as shown in Fig. 1. The cell consists of circular drive and sense coils collocated in an alumina-oxide ceramic torroid with 4.6-cm outer diameter, 2.3-cm inner diameter, and 4.6-cm axial length. The cell is filled with oil and capped by a flexible membrane to provide pressure compensation. A 2-kHz signal is applied to the drive winding, which is inductively coupled to the sense coil through the water path whose electric field is a torroid passing through the center hole of the ceramic housing. The output signal voltage is proportional to the conductivity of the water path, and is converted to a DC signal by in-phase sample-and-hold circuitry. The output is also dependent upon the resistance and inductance of drive and sense windings, which vary with pressure, temperature, and the magnetic properties of the winding core. A feedback loop technique greatly reduces these secondary factors. Three reference resistors are switched in by the ALACE controller to provide a ratiometric output proportional to conductivity. While the measurement is most sensitive to the water path through the hole, the field external to the coil housing plays a role so that external dimensions within 10 cm of the coils must remain unchanged to maintain 0.01 stability.

The ALACE controller uses a Motorola 68HC11 microprocessor configured with 32k ROM for program code plus 16k RAM for data storage and manipulation. The 68HC11 is programmed in FORTH, allowing a small kernel size and compact program code. A 32-kHz clock with a variable output-pulse period (ranging from 2 to 2048 s) is used to wake the 68HC11 from its low power mode, providing an overall 20-μA quiescent current for the majority of the ALACE operation, increasing to 12 ma during data acquisition and processing. The analog *C, T,* and *P* channels are multiplexed to a 12-bit analog-to-digital converter that burst samples and averages 100 readings to produce a sample with 14-bit resolution. Each variable is burst sampled every 2 s, stored in RAM at 14-bit resolution, and subsequently averaged into predetermined depth bins, typically ranging from 2 to 20 m in extent, for data transmission.

P-ALACEs use System Argos for data transmission. This forces us to degrade the precision of reported *T* and *S* and constrain the number of depth bins. Temperature profilers report 104 depth bins, while CTD profilers use 56 bins. The profile data are packed with other engineering data into four 32-byte Argos messages. Each of the four messages contains a different section of the profile. The data are packed by first-differencing each section and the differences are scaled to one of sixteen preset ranges to maximize resolution for a fixed number of output bits. Since in typical ocean environments 90% of the conductivity signal is due to temperature, *C* is stored after removing a preprogrammed quadratic *T* dependence, leaving primarily the salinity signal. Using these algorithms, data are sent through Argos using 6 and 8 bits for each *C* and *T* depth-bin reading, respectively. During postprocessing the *T* signal is used to reconstruct *C* and then to calculate *S.*

Sherman (1992) has described Argos throughput from ALACE platforms and this description applies to both the P-ALACE and the SOLO described below. Briefly, sparse satellite coverage means that only about 6% of transmitted messages are received (more at high latitudes, less at low latitudes, and less when there are many transmitters within the satellite footprint). Of the messages acquired, 9% contain at least one bit error, and these errors have the characteristics of long noise bursts rather than the random single-bit or short duration errors for which error correction is effective. P-ALACEs and SOLOs use Service Argos IDs that allow one message to be sent every 90–120 s. They use a rotating buffer to store and transmit in sequence the four messages needed to describe the full depth range of profiling. To achieve a high probability that all four messages are

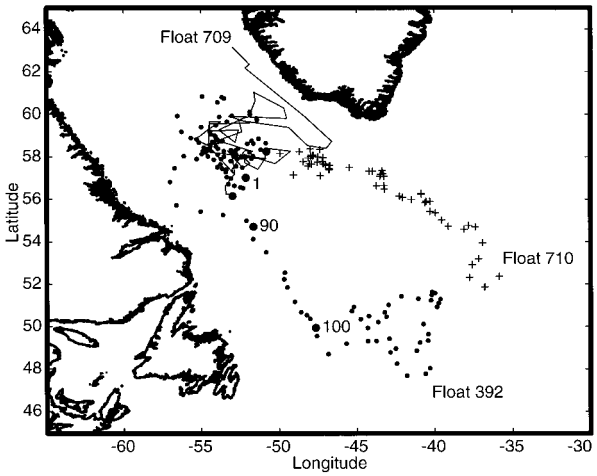

FIG. 2. Tracks of three floats in the Labrador Sea. Float 392 (small dots) starts at the large dot labeled 1. Between profile 90 and 100 (as marked) it advects out of the Labrador Basin. Floats 709 (line) and 710 (+) were deployed near the same location as 392 (first positions are marked by large dots) but 1 yr later.

successfully received, transmission extends over a 24-h on-surface period before the next cycle begins.

At typical ascent rates of 10–20 cm s^{-1}, the FSI cell flushes 99% of its volume every 10 cm so the effective time constant of the inductive cell results mainly from the size of the water volume over which the cell integrates. This should lead to a time constant of 0.5–1 s at typical ascent speeds, only slightly shorter than the temperature sensor timescale. The FSI sensor draws 70-mW power and is powered continuously during the ascent, requiring ~0.5 kJ for a 1-km profile. This consumes about 3% of the total P-ALACE or SOLO stored energy (see section 4).

Long-term deployments using the FSI cells have met with mixed results. Three representative floats, all deployed in the Labrador Sea, are discussed here. Their data are compared with shipboard CTD measurements taken in summer 1995 and fall 1996 from the R/V *Hudson* (courtesy of J. Lazier of the Bedford Institution of Oceanography). Plots of the *Hudson* data in the Labrador basin for both years indicate a reasonably tight θ versus S relation $S = 34.84 + 0.10(\theta - 2.9°C) \pm 0.01$ for data averaged between 800- and 1500-m depth. This relation was used to examine conductivity sensor performance by calculating S^*, the apparent salinity at 2.9°C. To minimize the effect of small-scale structure and error, θ and S for each profile were averaged over the range 800–1500 m and S^* was obtained by extrapolating the average salinity $\langle S \rangle$ from its average temperature $\langle \theta \rangle$ to 2.9°C using the slope $dS/d\theta$ of the θ–S relationship. For floats in the Labrador basin with accurate conductivity sensors, the time series of S^* should be constant to 0.01. The adjusted average salinity S^* is shown in Fig. 3a for float 392, in Fig. 4a for two other floats discussed in detail below, and in Fig. 4b for all floats deployed in the Labrador Basin.

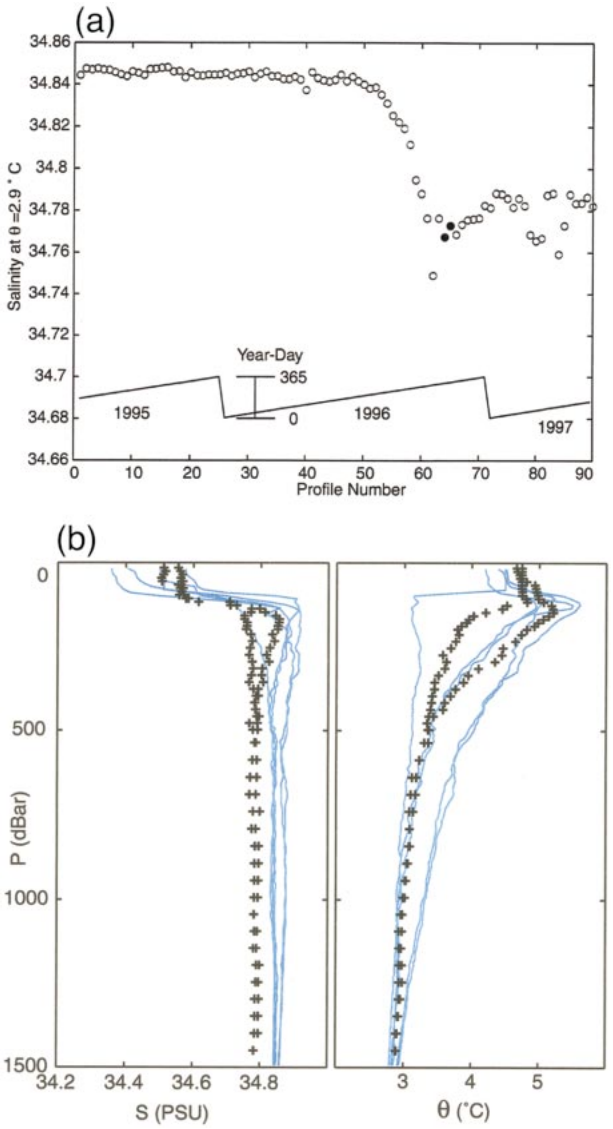

FIG. 3. (a) Here S^* is the average salinity between 800- and 1500-m depth adjusted along the θ–S curve to $\theta = 2.9°C$. The S^* values are shown for the first 90 profiles from float 392 when it was in the Labrador Basin. The corresponding yearday is the inset line plot. Profiles 64 and 65 (solid circles) are compared with shipboard CTD profiles in Fig. 3b. (b) Solid lines are a subset of CTD stations (courtesy of John Lazier) from a transect in Nov 1996 extending from 60.5°N, 57.3°W to 58.7°N, 54.7°W that passed within 100 km of float 392. Pluses are from 392's profiles 64 and 65 near 59.7°N, 53.9°W. The float's conductivity sensor had shifted ~0.06 psu fresh by this stage (see Fig. 3a).

Float 392, which had no biocide coating, executed 134 cycles from 1995 to 1998, profiling once every seven days, and left the Labrador basin in mid 1997 (see Fig. 2). The S^* time series, shown in Fig. 3a, for the first 90 cycles, while the float stayed in the basin, is stable to within 0.01. During the summer of 1996 and continuing into the fall, S^* drifted 0.06 fresh and then apparently stabilized again. This may indicate slight bi-

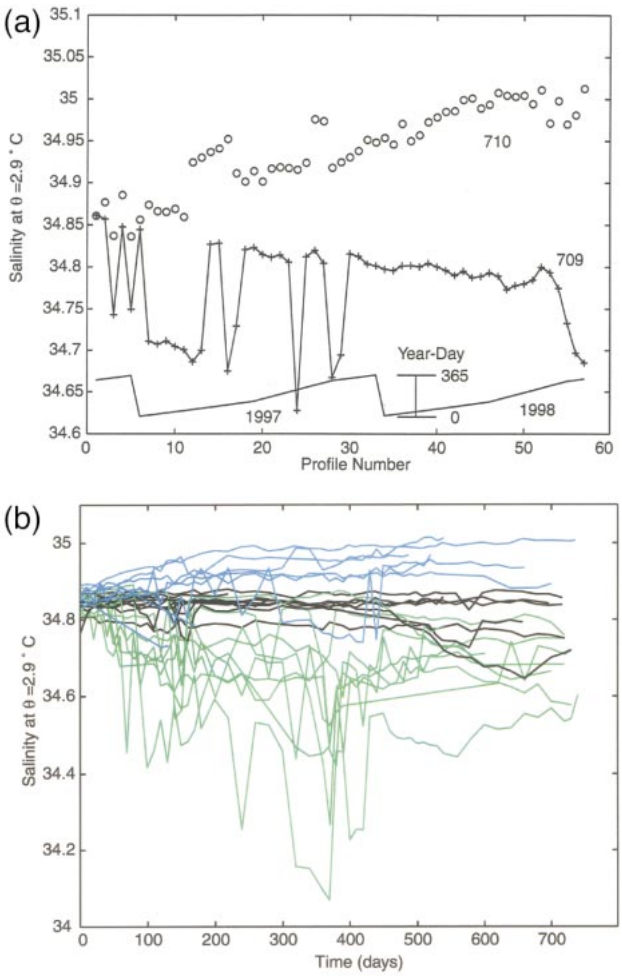

FIG. 4. (a) As in Fig. 3, *S** for float 709 (+) and 710 (o) with yearday inset below. Float 710 has antifoulant, which ablates over time causing apparent *S* to increase. The conductivity cell on float 709 jumps intermittently. (b) The *S** for 27 floats deployed in the Labrador Basin in 1996. Data are shown only for floats west of 40°W between 50° and 62°N. Time is days since deployment. Blue lines are for floats coated with an antifoulant. Green lines denote uncoated floats with *S** jumps of at least 0.1 psu between consecutive profiles; a large subset of the floats display this intermittent behavior. Black lines show well-behaved uncoated sensors.

ological fouling during summer that then stayed attached (e.g., barnacles). The *Hudson* CTD section stations in November 1996 passed within 100 km of float 392. Shipboard profiles moving from NW to SE of the float are compared with the float data in Fig. 3b. The CTD data show considerable along-transect structure in *T* with much less variability in *S* below 500 m. While float *T* profiles are bracketed by the shipboard data, float *S* is approximately 0.06 fresh, consistent with the observation in Fig. 3a that the float's salinity calibration had shifted by this time.

The track of float 709, which cycled every 10 days in the winter and every 20 days during summer, is also shown in Fig. 2. The *S** trace, shown in Fig. 4a, exhibits abrupt "jumps" of 0.15 on several occasions. Sometimes the sensor jumped from erroneous to apparently proper values inside a single profile to produce a step in measured *S*. From diagnostic data taken just prior to ascent, it is evident that readings jumped either because the cell itself shifted or something in the cell drive or sense electronics changed because amplifiers and analog-to-digital conversion were shown stable by telemetered test data. The jumps cannot be explained by errors in *T*, which showed no associated jumps.

Over the 2-yr span, measured salinity from float 709 also gradually freshens by 0.05, with a larger drift of 0.2 over the last few profiles. The conductivity cell on float 709 had no biocide coating so the long-term drift to fresher values, particularly the slow drift over the majority of the record, are likely to be the result of biofouling, reducing the cell-opening cross section. The more rapid drift at the record's end may be associated with the same problem that induces jumps. Float 710 (also shown in Fig. 4a) shows the effect of biocide washing away as *S** drifts 0.15 higher over the 2-yr period. Of these three floats, only 710 had biocide applied to the cell. As the coating diffuses away, the cross-sectional area of the hole in the sensor increases, raising the estimated conductivity and producing a long-term rise in *S*. For the FSI cell geometry, losing 25 μm of coating would cause *S* to increase 0.15.

The 2.9°C equivalent salinity *S** was calculated for all CTD floats released in the Labrador Sea in 1996 while they were in the area west of 40°W and between 50° and 62°N where the θ–*S* relationship is reasonably constant. The resulting time series (Fig. 4b) are all well represented by the three cases above: all cells where *S** drifted higher had antifoulant; most cells without biocide drifted to lower *S**; some cells remain stable; and quite a few are very noisy. Of the seven floats with biocide, six drift higher before generally stabilizing after ~200 days with a 0.1–0.2 increase of *S**; the seventh cell with biocide suffered from noise. At the end of data collection within the selected region, 8 of 20 of the cells without biofouling had *S** within $\pm$0.05 of their start values and 12 were at least 0.05 fresher. Of the 12 untreated floats remaining in the region after 700 days, 3 kept *S** within 0.05 of their starting value while 9 drifted at least 0.1 fresh. Over 50% of the floats experience at least one jump of *S** greater than 0.1 psu between consecutive profiles. Although the *S** diagnostic could be refined using more elaborate θ–*S* curves that are functions of locale and season, this will not change the conclusion that both treated and untreated cells were subject to significant drifts and instabilities, probably for different reasons.

The antifoulant applied to these early P-ALACE conductivity sensors is a hard vinyl, nonablating formula (Z-Spar P-33). Although the paint itself does not wash away, the poisons do leach out over time causing the antifouling coating to become thinner. That the painted cells ceased drifting toward higher *S* (as in Fig. 4b after

200 days) is probably an indication that all of the biocide has leached away. On later floats FSI applied a different antifouling compound that behaved in the same way. On the new SOLO float described below we have also installed Sea-Bird Electronics (SBE) three-electrode cells that require a seawater pump to achieve reasonable flushing times. While this uses extra power, pumping is an advantage when it comes to avoiding biofouling because between measurements the water in the conductivity cell is stagnant. Then poison tablets located at the entrance and exit of the cell allow biocide concentration to become high without rapidly depleting the poison, thereby potentially providing years of protection. Such an approach works only when the electric field is completely contained and is not affected by the changing dimensions of the biocide tablets as they slowly dissolve. We have carried out only preliminary tests of the SBE sensor but S. Riser (1999, personal communication) reports good results after more than a year using a similar cell installed on P-ALACE floats.

In summary, the FSI conductivity sensors with which we have the most experience were subject to both drifts and abrupt jumps in calibration. Cells with antifouling coatings drifted smoothly toward higher conductivity at a rate that was fairly uniform between floats. We attribute this to ablation of the biocide coating that changed the effective dimensions of the cell. With a stable θ versus S relation at some measured depth, this drift should be correctable, and in the Labrador basin was corrected to a salinity error near 0.01. Some cells that were not treated with biocide drifted very slowly while others drifted as rapidly as the treated probes, albeit in the opposite direction. We attribute this to biological growth on the sensors changing their effective dimensions. Such data should also be correctable to an accuracy near 0.01 given a stable θ versus S relation.

The more serious conductivity problem was abrupt jumps in calibration that, in our experience, usually signaled that subsequent data were unusable and uncorrectable. These are not related to errors in digitization or in sensing temperature. We believe that because the jumps are of both signs, are of a relatively uniform magnitude, and are closely tied to specific instruments, they cannot be blamed on impact with biological particles or other forms of biofouling. The manufacturer has reported discovering two intrinsic problems with conductivity sensors that may have caused the jumps seen in this study. A problem gluing the ceramic housing (the torroid and stem) of some cells might have allowed water to enter the cell, effectively changing its geometry. An occasional instability in a low-level amplifier (a problem not eliminated until after all the floats here were deployed) is reported to cause calibration changes not dissimilar to those seen here. Since these difficulties have subsequently been solved, it is expected that more recently manufactured sensors will not exhibit these jumps.

3. Measuring vertical velocity

Voorhis and Webb (1970) placed horizontal propeller blades around the vertical axis of a subsurface float to create a Vertical Current Meter (VCM). Relative vertical flow past the VCM caused it to rotate and this rotation was telemetered through the acoustic signal used to track the float over days. Because a float follows horizontal flow, there is no relative horizontal velocity to contaminate the vertical velocity measurement the way horizontal flow contaminates the vertical velocity of a misaligned sensor on a mooring. We have developed both P-ALACE and SOLO versions of the VCM to gather long time series of vertical velocity as part of the Labrador Sea Deep Convection Experiment (Lab Sea Group 1998). To do this we replaced the standard stability disk (see Fig. 9) with a 6-blade propeller (0.64-m outer diameter) that uses the float's vertical axis as an axle. The blades themselves have the shape of a flat plate with rounded leading and trailing edges. The blades have a pitch angle of 20° with respect to the vertical, resulting in a full rotation for every 4 m of net relative vertical motion. This pitch, lower than used previously, was selected to minimize hydrodynamic stalling that would cause the calibration between rotation and relative vertical velocity to differ from that for an unstalled blade. Lift on the blades is required to produce the torque needed to accelerate the float's rotation rate. If this occurs when the relative velocity itself is low the blades will stall. Reduced pitch both reduces the amount of angular acceleration needed to follow a change in w and reduces the lift required to produce a given torque. Consequently, reducing the pitch to half its customary value almost halves the range of relative velocity over which stalling occurs.

Net rotation R is accumulated by summing every 8 s the changes of float orientation measured by an internal compass (Precision Navigation, Inc. model Vector 2X). While the float is drifting at its neutral buoyancy depth, time series of P, T, C, and R are collected over an 88-h period with 0.5-h time resolution using the instrumentation described above. Time series are first-differenced, scaled to one of 16 preset ranges and encoded using 5 bits per datum. After the VCM ascends, two Argos IDs are used to transmit profile and time series data in a total of 512 bytes (8 messages for each ID). Even at the high latitude of the Labrador Sea, where Argos coverage is good, some messages are not correctly received during the 24-h transmission period, implying that the maximum Argos throughput is ~250 bytes per day per ID, in substantial agreement with Sherman (1992).

Since the rotational response time is short compared with the timescale expected for w, the float rotation, dR/dt, measures the relative velocity between the vertical water velocity, w, and the float's vertical velocity, w_F, according to

$$dR/dt = \gamma[w - w_F] = \gamma[w + (1/g\rho)dP/dt], \quad (2)$$

where the float's velocity has been related to its pressure change, dP/dt, using the hydrostatic relation. Absolute vertical velocity is calculated from telemetered data using (2). This procedure makes no assumption about the cause of the float's vertical velocity.

The constant γ relating dR/dt and relative velocity can be estimated using pressure changes and rotation during surfacing cycles by assuming that w is small compared with the rate of depth change. This shows γ to be constant, as expected. This calibration procedure is accurate to a few percent but is not sensitive enough to detect potential small errors like underresponse at low speeds or an asymmetric response to up and down motion that might result if the propeller is more influenced by the instrument wake in one direction than the other.

In addition to direct measurements, vertical velocity is inferred from temperature T according to

$$w_T = w_F - (dT/dt)/(\partial T/\partial z)_o, \qquad (3)$$

where the time derivative is taken following the float, w_F is inferred from pressure, and $(\partial T/\partial z)_o$ is averaged over the two profiles bracketing the time series. Errors in w_T arise mainly from lateral advection of T by highly sheared intrusive or frontal flow with scales smaller than the float (the float follows horizontal flow on its own scale) and because $\partial T/\partial z$ varies with depth and over the 88-h time series. For comparisons the vertical displacements η, the time integral of measured w, and η_T, the integral of w_T, are useful.

The accuracy of vertical velocity measurements is investigated using two VCM P-ALACEs deployed in October 1996 off California. Both floats drifted at 700 m for the first cycle, readjusted their ballasting to follow a 500-m target and proceeded to drift at 500 m for their remaining cycles. Their missions for this engineering test were to repetitively execute four cycles in VCM mode (a T profile plus w, T, and P time series accumulated over 88-h at-depth periods were observed) and one cycle in profile mode (where only the profile was reported).

The two floats, serial numbers 580 and 581, were deployed within 2 km and 0.5 h of each other and after their initial cycle surfaced within 2 km of each other. The resulting displacement time series from this first cycle, shown in Fig. 5, disclose a significant internal tide, a strong persistent downwelling of $O(0.3\ \text{mm s}^{-1})$ and good agreement between the two floats and between η and η_T. The standard deviations, σ and σ_T, of η and η_T around best-fit linear-in-time means were computed for each 88-h time series and averaged over the 2-yr span. The ratios σ/σ_T for the two floats were 0.96, 1.04.

Vertical velocity has often been inferred from measurements of T at a single point coupled with an estimated mean gradient $(\partial T/\partial z)o$ as in (3). Like our use of (3), this method neglects fine structure variation of the vertical gradient. It also neglects lateral advection on all scales. When this method is applied to moored measurements, fine structure features advected past the sensor by the larger scale internal wave field result in contaminated spectral estimates. If a time series of temperature profiles is available, isotherms can be tracked and errors from linearizing vertical advection eliminated (Pinkel et al. 1987), but contamination from Doppler-shifted, horizontally advected fine structure remains. A VCM drifts with the local horizontal velocity, minimizing horizontal-advection contamination, but, unless the float follows isotherms, wT still suffers from contamination by vertically advected fine structure. However, the high vertical coherence of isopycnal displacements (Pinkel et al. 1987) indicates that there is little w energy at high vertical wavenumbers so direct measurements of w by VCMs should have minimal fine structure contamination.

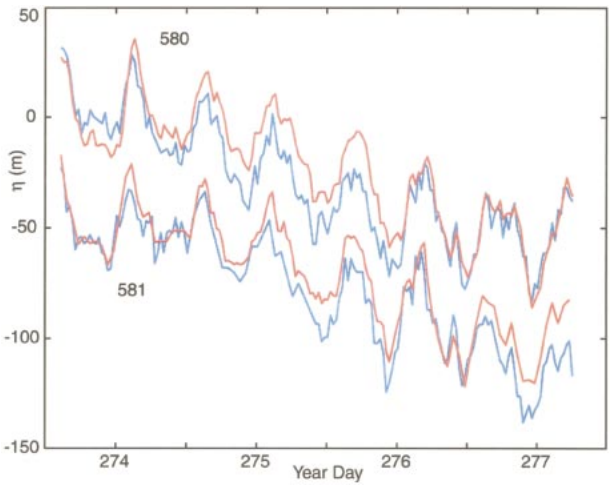

FIG. 5. Vertical displacements for floats 580 (upper traces) and 581 (lower) that were deployed at the same location within 0.5 h. Traces for float 581 have been offset. Blue lines are η from VCM rotation while red lines are vertical displacement η_T determined from temperature. Over the 88-h period the internal tide and an overall downwelling of $\sim$0.3 mm s^{-1} (24 m day^{-1}) dominate.

Average w spectra were computed from the complete series of floats 580 and 581 using a Blackman window. Data from a region of high, apparently eddy-related variability, south of the Channel Islands and a period of grounding along the central California continental slope (see Fig. 6) were excluded. The spectra, shown in Fig. 7, begin at a floor below 0.02 cph, rise roughly as ω^2 from zero through the inertial frequency f, reach a peak at the lunar semidiurnal tidal frequency M2, and then drop to a white spectral level at high frequency. The spectra agree well with those that Pinkel et al. (1987) measured by tracking isopycnals and with the Garrett-Munk GM79 empirical model (Munk 1981), with its $(\omega^2 - f^2)^{1/2}/\omega$ spectral dependence, except that the GM79 is missing the M2 peak. The VCM spectra show more leakage below f, perhaps due to averaging over a range of latitudes or the effect of the relative vorticity

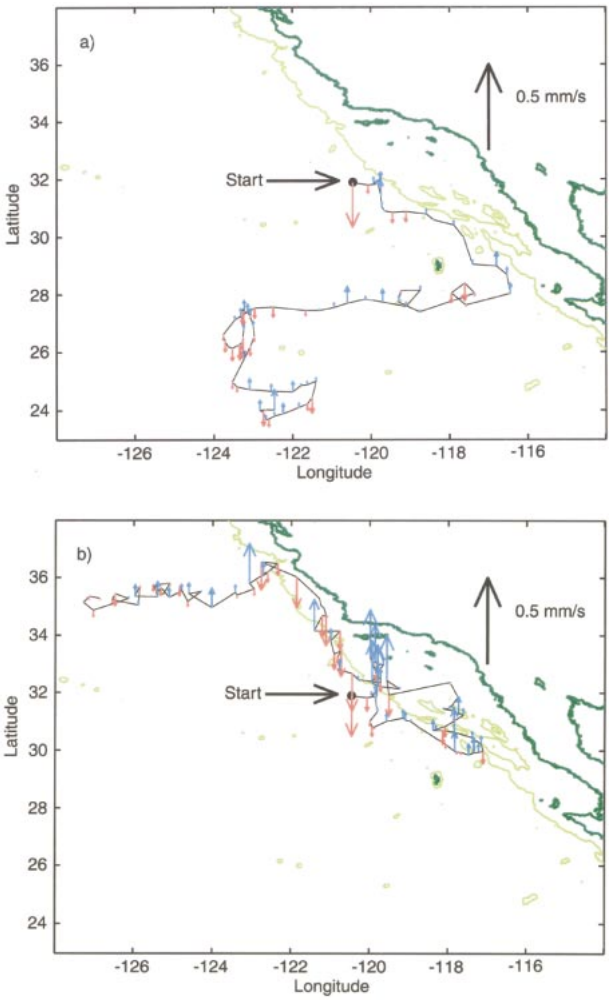

FIG. 6. Trajectories of VCMs (a) 580 and (b) 581 with deployment site marked by a dot. Both drifted south to 30°N. Then 580 looped back to the north while 581 went between Guadelupe Island and Baja California and then westward. Arrows show averages of the measured w over each 88-h cycle (red for downwelling, blue for upwelling). The 2000-m isobath is light green. Generally, strong vertical velocities are associated with the central coast and Channel Island area where mesoscale eddies are energetic.

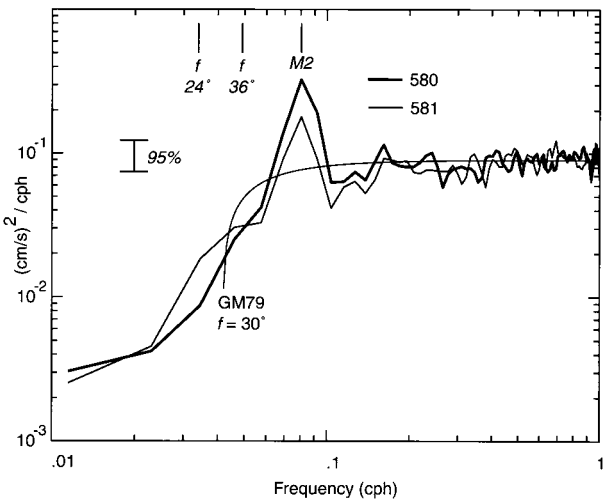

FIG. 7. Vertical velocity spectra from VCMs 580 and 581 compared with the Garrett–Munk '79 model. The GM79 model shown is for f at 30°N. The floats ranged over 24°–36°N with the resulting range of f marked at the top.

on mesoscale features. It is encouraging that these directly measured w spectra present no surprises.

The evidence above suggests that VCMs respond well to the typical vertical velocities of internal waves. How well do they measure the weak vertical velocities associated with phenomena like mesoscale eddies and coastal and equatorial upwelling? Here a small asymmetric response could significantly bias w and even typical relative vorticities turning the float (each rotation implies 4-m vertical displacement) must be considered a potential error source. Figure 6 shows the trajectory of floats 580 and 581 and the average w for each 88-h segment along their trajectories. Float 581 moves southeastward to about 28°N and then turns southwestward as it joins the equatorial branch of the subtropical gyre. Float 580 follows 581 to about 30°N then reverses to move northwestward along the coast until heading westward off of Monterey Bay. It sees high w, and high variance of w and w_T, south of the Channel Islands. There is a local maximum of eddy variability in geostrophic sea surface currents in this region disclosed by TOPEX/Poseidon altimetry and we tentatively ascribe the large observed w variability to these eddies. This float also grounds along the continental slope near 35°N, off the central California coast. Grounding introduces spurious ''vertical velocity'' signals, and, since it is difficult to tell when grounding occurs, we cannot investigate the near-bottom upwelling that one would expect to accompany the grounding of a current follower.

To more closely examine low-frequency vertical motion, the 88-h time series of η for each float were joined together by setting the average η value over the first 12.5 h of one cycle equal to the average over the last 12.5-h average of the previous cycle; a 12.5-h period minimizes aliasing of tidal signals. In this the grounding periods for float 580 near day 700 (day of 1996 extended) were skipped and the vertical displacements held fixed across the gap. Except very near bathymetry we expect temperature to be reasonably conservative and therefore use η_T as a standard for testing the VCM measurements. Based on the basic symmetric calibration, the low-frequency displacements η for both floats showed a general upwelling of 2–3 m day^{-1} for which there was no analog in η_T. This mean upwelling is much greater than could be explained by anything but an asymmetric response to upward and downward flows. Figure 8 shows the joined series of η calculated by assuming that the rotational response to upward flow is 2.5% greater than to downward motion. Also shown are series of η_T joined in the same way as η.

Over the first 50 days the two floats give nearly iden-

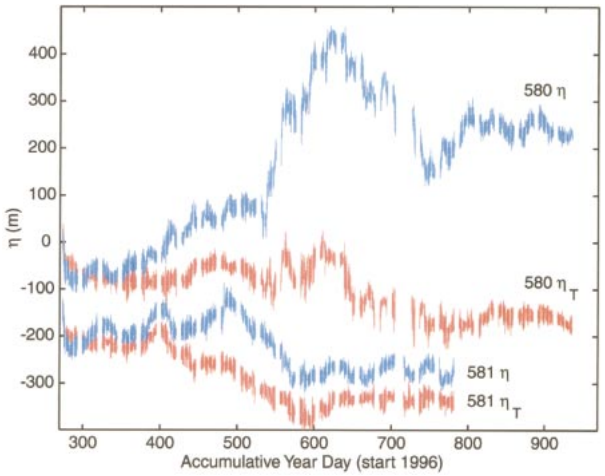

FIG. 8. Time series of η (blue) and η_T (red) accumulated over 2 yr. Float 581 values are offset by -150 m. Gaps every $\sim$20 days result from a one-cycle programmed change out of VCM mode. The gap for float 580 near day 700 results from the float grounding off the California central coast.

tical η time series. They also give nearly identical η_T series, but these η_T series differ from the directly measured η series, missing, for example, the approximately 30-m rise in η around day 320. For float 581, which drifted southward, there is a general similarity between η and η_T throughout the measurement period although the directly measured η has more structure, both in the first 50 days as noted above and throughout the record. The chosen asymmetry correction brings the mean w and w_T for float 581 to within 0.1 m day^{-1} while float 580 shows a net upwelling w of O(1 m day^{-1}) that is not mirrored in w_T. For float 580 there are features on the 30–50-day timescale that correspond between η and η_T, but the directly measured signal again has more structure. The discrepancies between η and η_T early in the record that are reproduced in each float points to the serious errors that can result from neglecting horizontal advection and fine structure when inferring w from isotherms.

How well can the VCM measure the large-scale pattern of upwelling? To get errors below O(3 m day^{-1}) it will be necessary to account for up/down asymmetry. As demonstrated by the difference in the net upwelling observed by our two floats, it may be necessary to calibrate each float to 0.5% to get calibration errors below O(1 m day^{-1}). Beyond this, there are features seen in float 580, notably between days 550 and 725, that differ between w and w_T at the O(1 m day^{-1}) level but cannot be easily explained with calibration. There is generally extra structure on the 10-day scale seen in directly measured w over that inferred from temperature. Over the first 100 days, while the floats are close, η agrees between the two floats but disagrees with η_T at the O(3 m day^{-1}) level. This suggests that the extra structure of directly measured w is not instrumental and implicates relative vorticity in inducing float rotation not related to w. It remains uncertain how well we can count on temperature to mark material surfaces but we think it unlikely that the observed differences of w and w_T result from using temperature rather than potential density as a conserved tracer. We therefore conclude that even if long-term drift is used to establish accurate asymmetric calibrations, signals at the O(1 m day^{-1}) level cannot be measured and that errors of up to O(3 m day^{-1}) level are possible over limited time periods.

4. The SOLO design

The Sounding Oceanographic Lagrangian Observer (SOLO) is a second generation subsurface float using the same operating principle as the original ALACE float: it repeatedly cycles between depth, where measurements are made, and the surface to allow satellite tracking and data relay. Design objectives for the SOLO were to increase operational flexibility by allowing full depth control, to eliminate recurrent failures associated with air in the ALACE hydraulic system, to increase energy efficiency, and to produce a more robust instrument capable of air deployment. These led to replacing ALACE's reciprocating high-pressure pump and fragile internal reservoir with a buoyancy engine based on a single-stroke hydraulic pump with a small air pump used to generate extra buoyancy at the surface. One of the major benefits of the single-stroke piston is the ability to accurately increase or decrease buoyancy at high pressure, thus allowing the float to actively seek either a desired depth or isotherm, or to perform multiple profiles between subsurface depths before returning to the surface. This added flexibility allows the SOLO to perform a larger variety of scientific tasks than the ALACE could. This same general approach is also being taken by Webb Research Corp. in its APEX float (S. Riser 1999, personal communication).

The SOLO hydraulic system consists of a single-stroke piston driven by a ball screw and motor, which pushes oil into an external pillow bladder, located at the bottom of the float (Fig. 9). Because the external bladder is never emptied of oil, it always sees the external pressure and the float's pressure port is placed in this part of the hydraulic system. Because high pressure hydraulic pumps are inefficient at low pressure, a separate pneumatic system is used to efficiently generate surface buoyancy to ensure that the float tracks the water surface well and maintains good antenna height even in rough sea states. This is accomplished with a small air pump and valve that move 1 L of air from inside the pressure case into a sleeve bladder that surrounds the main float tube. The hydraulic and pneumatic bladders are both made by the Goodyear Rubber Company of a proprietary nitrile-rubber compound. The hydraulic bladder is built using a blind-mold process while the sleeve bladder is built using mandrel lay-up.

The SOLO reaches its neutral-buoyancy pressure, P,

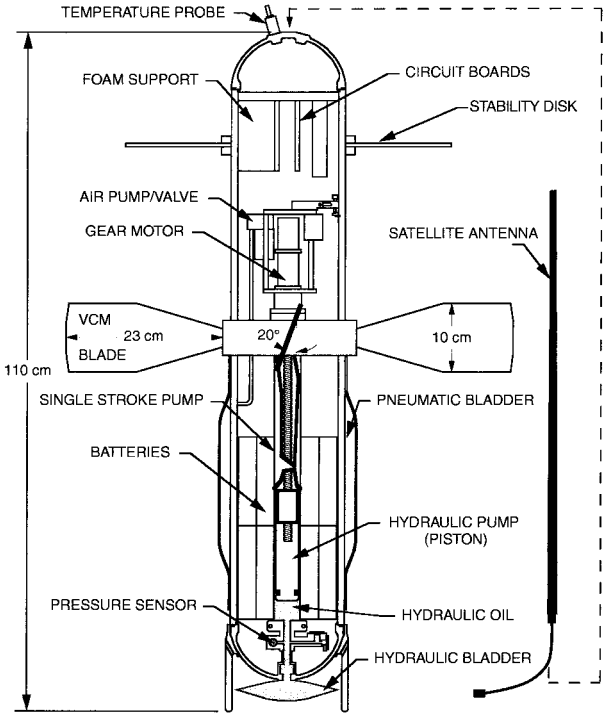

FIG. 9. The SOLO is a second generation float incorporating a rugged single-stroke pump for full depth control. A pneumatic pump fills the external sleeve bladder to provide 1 liter of extra surface buoyancy at low energy cost. Also shown is the propeller used to measure vertical velocity that has the same configuration for P-ALACE and SOLO VCMs. An FSI conductivity sensor is sometimes mounted as shown in Fig. 1. Sea Bird CTDs are also sometimes mounted on the instrument axis above the top cap.

when its mass, M_o, equals that of the water displaced, that is, when

$$M_o = \rho(P, T, S)[(V_o + \delta V)(1 + \alpha T - \gamma P)], \quad (4)$$

where ρ is the local water density, V_o is the float's volume ($\sim$23 L) at $T = P = 0$, δV is the volume of oil displaced externally by the pump, α is the float's thermal expansion coefficient, and γ is its overall compressibility. If a float had the same compressibility as seawater it would approximately track isopycnals but SOLO's 6061-T6 aluminum pressure case is less compressible than water so that the float tends to settle out on isobars, although it is still influenced by ρ. The total volume that can be displaced by the hydraulic pump, $\delta V_{\max}$, must provide enough buoyancy to raise the SOLO to the surface. For the world's oceans this is a concern where the warm surface waters are the least dense (the equatorial ocean) or where the surface waters are much fresher than those at depth (e.g., Mediterranean Sea and Bay of Bengal). Two SOLO pumps have been designed to displace 140 and 200 cc's of oil. The smaller pump allows a smaller, lighter float that can return from 750-m depth in almost all regions of the world and from 1500 m in most areas. The larger pump provides a 1500-m depth range in all but the most stratified waters.

Experience with the ALACE pointed to intermittent hydraulic failures when the ALACE misses cycles by failing to pump enough oil to get to the surface. One suspected failure mode is sensitivity of the high pressure solenoid valve or of the valves in the reciprocating pump to contaminants. Another is air in the hydraulic system. The ALACE pump has a relatively low compression ratio (ratio of volume above the piston at minimum and maximum compression) so that if the compressibility of the hydraulic fluid is raised by air bubbles, the peak pressure produced in the pump may fail to reach the ambient pressure and pumping will cease. The SOLO pump has no valves to be contaminated and it has a high compression ratio. Bench testing shows that the pump continues to operate at high pressure and over several hundred cycles, even with contamination levels much higher than are expected from normal assembly and even with a significant fraction of air in the hydraulic fluid.

The critical part of SOLO is its hydraulic pump. Because hydraulic oil leaking to the low-pressure side of the piston is a potentially fatal failure mode, construction of the cylinder, piston, and the seal between them is very important. The piston and cylinder are machined from 7075-T651 aluminum. The cylinder is gun-bore drilled, honed, anodized, coated with a proprietary sealant HardTuf X20, and rehoned to the specified diameter. An elastomeric nitrile tee-seal with adjacent support rings is used to provide high pressure integrity between the piston and cylinder.

Due to the high gear reduction of the motor and friction of the seal and bearings in the piston, the single-stroke piston has a moderate efficiency. It is, however, high enough that a simple latching brake is needed to keep the imposed pressure from driving the pump and motor when power is removed. Multiple measurements show the overall efficiency, comparing the output power (flow rate times pressure) to the input electrical power, to be 30%–40% for pressures >1000 db (Fig. 10). A complete ascent operation involves a high pressure displacement of 200 cc at depth (sometimes split between more than one depth) and delivery of 1 L of air by the pneumatic pump into the sleeve bladder upon reaching surface. For descent, air in the sleeve bladder is released back into the float under its own pressure and the piston is retracted. Since most of the buoyancy is provided by the high efficiency pneumatic system, the energy required for a complete cycle is less than for the ALACE system, while producing $\sim$60% more surface buoyancy (1200 cc for the SOLO vs 750 cc for the ALACE).

The SOLO battery pack consists of 16 DD Lithium cells, which, after derating to 66% for cold temperature and longevity, yields 80 A-h at 14V or the equivalent of 4 MJ. For a 1000-m depth cycle, the energy budget per cycle is:

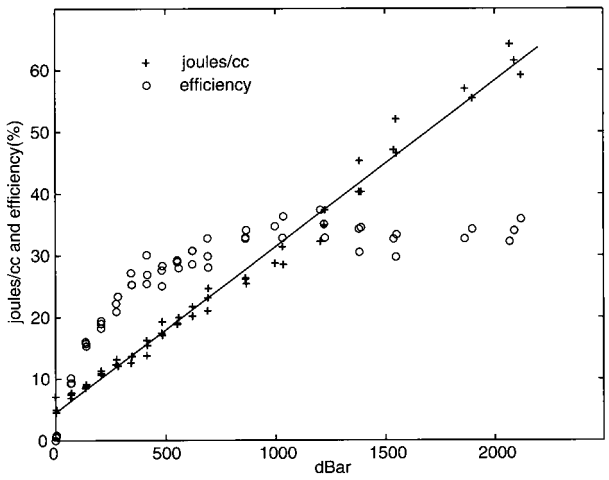

FIG. 10. Overall efficiency of the single-stroke pump and motor (o) is ~32% at high pressure. The amount of joules required to pump 1 cc (+) is a linear function of pressure (solid line is a least squares fit: J cc^{-1} = 5 + 0.027 P db^{-1}).

Hydraulics	7.4 kJ
Pneumatics	0.4 kJ
Argos	10 kJ
Other	0.5 kJ
Total	18.3 kJ

A standard SOLO should be able to execute at least 200 cycles to 1000 m with its stored energy.

The sensors, controller, data storage, and method of transmitting data through Argos are the same as used in the P-ALACE.

5. Conclusions

Autonomous Lagrangian floats that were developed to track subsurface currents are also natural platforms for gathering profile and time series data. As more sophisticated sensors are implemented there is a heavier demand for a reliable float that can carry out more vertical cycles and employs sensors that are accurate over extended periods of operation. The Sounding Oceanographic Lagrangian Observer (SOLO) is a second-generation design designed to provide these characteristics. It incorporates a robust hydraulic system to increase reliability. With its single-stroke piston comes the flexibility for active two-way depth control and the ability to track not only isobars but any property, like temperature or density, that can be sensed.

Obtaining a conductivity sensor that matches the longevity of the floats has met with mixed results. Diagnosing in situ sensor problems is difficult, as floats are rarely recovered. Biofouling is a central concern and H. Freeland (1998, personal communication) observed severe fouling on a P-ALACE recovered near OWS P. However, biofouling is not the only story (see Fig. 4a, float 709). Sensor manufacturers are confronted with large obstacles of overcoming fouling, operating on low power, and providing long life and reliability. The task has not yet been finished.

Floats outfitted with vanes, designed to measure deep convection events in the Labrador Sea, demonstrate the ability to track internal waves as well as the lower magnitude velocities associated with coastal and equatorial upwelling (Fig. 5). Estimates of asymmetry in the response to w point to bias errors of 2–3 m day^{-1}, that can be corrected given long time series. Short-term errors that cannot be explained by any consistent calibration problem are also observed. Data from two floats in a region where temperature should be reasonably conservative show consistencies both between floats and between vertical motion measured directly and inferred from temperature. This suggests accuracy on timescales of months near 1 m day^{-1} with errors of O(3 m day^{-1}) on timescales of a week.

New SOLOs under development include internally recording temperature microstructure floats (similar to LAMP; Sherman and Davis 1995) and SOLOs with three-channel optical irradiance sensors and beam transmissometers. These and future floats will be able to reap the benefit of much better satellite locating and communication capabilities that will remarkably improve the data bandwidth, allowing more data to be relayed more quickly. This will support higher measurement resolution, greater depth resolution, and more sensors. It is also hoped that reducing the time spent at the surface will also reduce the adverse effects of biological fouling on sensors.

Acknowledgments. The development of ALACE and initial versions of the P-ALACE were supported by the Office of Naval Research under several grants. The SOLO was developed by the Instrument Development Group of the University of California at San Diego. Initial SOLO testing, including early Labrador Sea deployments, and the profiling version depended on NOAA funding through Grant NA77RJ0453 and its predecessor. The development and deployment of VCM floats in the Labrador Sea was supported by ONR Grant N00014-98-10065 and its predecessor. Other deployments of profiling floats in the subpolar gyre, including the Labrador Sea, were supported by the National Science Foundation (Grant OCE95-31880) as part of the Atlantic Circulation and Climate Experiment. The prototype pneumatic sleeve bladder used in SOLO was developed at our request by Webb Research Corporation.

REFERENCES

Davis, R. E., 1998: Preliminary results from directly measuring middepth circulation in the tropical and South Pacific. *J. Geophys. Res.,* **103,** 24 619–24 639.

——, D. C. Webb, L. A. Regier, and J. Dufour, 1992: The Autonomous Lagrangian Circulation Explorer (ALACE). *J. Atmos. Oceanic Technol.,* **9,** 264–285.

——, P. D. Killworth, and J. R. Blundell, 1996: Comparison of Au-

tonomous Lagrangian Circulation Explorer and fine resolution Antarctic model results from the South Atlantic. *J. Geophys. Res.*, **94,** 855–884.
Fougere, A. J., 2000: New non-external field inductive conductivity sensor (NXIC) for long term deployments in biologically active regions. *Proc. of MTS/IEEE Oceans 2000 Conf.*, Vol. 1, 623–630.
Lab Sea Group, 1998: The Labrador Sea Deep Convection Experiment. *Bull. Amer. Meteor. Soc.*, **79,** 2033–2058.
Munk, W., 1981: Internal waves and small-scale processes. *Evolution of Physical Oceanography*, B. A. Warren and C. Wunsch, Eds., The MIT Press, 264–291.
Pinkel, R., A. Plueddemann, and R. Williams, 1987: Internal wave observations from FLIP in MILDEX. *J. Phys. Oceangr.*, **17,** 1737–1757.
Rossby, T., and D. C. Webb, 1970: Observing abyssal motions by tracking Swallow floats in the SOFAR channel. *J. Mar. Res.*, **17,** 359–365.
——, D. Dorson, and J. Fontaine, 1986: The RAFOS system. *J. Atmos. Oceanic Technol.*, **3,** 672–679.
Sherman, J., 1992: Observations of Argos performance. *J. Atmos. Oceanic Technol.*, **9,** 323–328.
——, and R. E. Davis, 1995: Observations of temperature microstructure in NATRE. *J. Phys. Oceanogr.*, **25,** 1913–1929.
Swallow, J. C., 1955: A neutral-buoyancy float for measuring deep currents. *Deep-Sea Res.*, **3,** 74–81.
Voorhis, A. D., and D. C. Webb, 1970: Large vertical currents observed in a winter sinking region of the northwest Mediterranean. *Cahiers Oceanogr.*, **6,** 571–580.